Check for updates

Adsorption-assisted decontamination of Hg(II) from aqueous solution by multi-functionalized corncob-derived biochar

Faheem, [ID] Jianguo Bao,* Han Zheng, Haseeb Tufail, Sana Irshad and Jiangkun Du*

Mercury (Hg) contamination of wastewater streams as a result of anthropogenic activities is a great threat to living organisms due to its acute toxicity. Therefore, current research is focused on the development of effective remediation technologies to protect human health and the environment. In this study, a novel chemical modification route was applied for the multi-functionalization of biochar in order to make it more efficient and selective for Hg(II) removal from aqueous solution. The amino-grafted modified biochar (AMBC) having multifunctional groups on its surface was successfully synthesized through the activation of excessively available carboxylic groups (−COOH) on pre-oxidized biochar (BC−COOH). The maximum Hg(II) adsorption capacity for the optimized amino-BC2 sample was 14.1 mg g^{-1}, which was almost twice as that for pristine biochar (BC, 7.1 mg g^{-1}). SEM, FTIR, and XPS techniques were applied for the confirmation of chemically grafted amino groups as well as the presence of residual −COOH groups on the biochar surface. Based on the batch adsorption data, adsorption kinetics and isotherms as well as XPS results, it was concluded that the Hg(II) removal mechanism was purely driven by chemisorption such as electrostatic interaction, surface complexation, ion exchange with no precipitation and crystalline material being adsorbed on the adsorbent surface. These research findings not only provide a suitable adsorbent for decontamination of Hg(II) from aqueous solution but also offer a new route for the multi-functionalization of biochar in order to make environment-friendly and inexpensive adsorbents.

1. Introduction

Heavy metals are the most critical pollutants in nature among all the industrial pollutants due to their non-biodegradable and bioaccumulating behavior.[1] Among all heavy metals, the unique nature of mercury, such as mobility and long residence period in atmosphere, facilitates its exposure to human beings, which results in many renal and neurological issues such as anxiety, loss of memory, loss of speaking and hearing abilities, cerebral palsy, and kidney and gastrointestinal problems.[2,3] Both natural and anthropogenic activities such as volcanic eruptions, rock weathering, biogenic emissions, chloralkali industries, metallurgical processes, electroplating, and wood pulping result in the release of highly toxic mercury into the environment.[4,5] Due to the acute toxicity of mercury, the US Environmental Protection Agency defines a maximum permissible concentration of total mercury as low as 10 μg L^{-1} for wastewater discharge and 2 μg L^{-1} for drinking water.[6] Therefore, the proper removal of mercury(II) from wastewater streams is necessary in order to produce effluents with acceptable quality for discharge into receiving water bodies or for their suitable and safe reuse in

land applications, otherwise these pollutants will directly or indirectly contaminate the surface as well as ground water, which causes health risks. Recently performed studies confirm the effectiveness of adsorption processes through carbonaceous materials such as biochar, particularly for low mercury metal concentration ranges in between 1 mg L^{-1} and 100 mg L^{-1} due to available oxygen functional groups (OFGs) and π electrons on the biochar surface.[7] Furthermore, it was proposed that Hg(II) sorption from solution was mainly subjected to two important mechanisms, *i.e.*, through a precipitation process and a reduction reaction due to the sharing of electrons.[8,9]

Biochar is mostly produced from agricultural and livestock waste, such as crop residue, wood chips, and animal dung, through pyrolysis. Pyrolysis is basically a thermochemical conversion of carbon-rich biomass into biochar, which has a higher surface area and a profound porous structure under an oxygen-limited condition at a temperature range of 300–1000 °C.[10] Despite having unique properties such as a large surface area and a porous structure, pristine biochar (BC) demonstrates a relatively low affinity towards targeted heavy metals. The reason is that low temperature biochars have relatively excess OFGs that may serve as the active sites or have an affinity for heavy metals ions sorption, while the high temperature biochars exhibit larger surface areas and more porous structures but fewer OFGs, so they have less affinity towards

School of Environmental Studies, China University of Geosciences, Wuhan 430074, P. R. China. E-mail: bjianguo@cug.edu.cn; dujk@cug.edu.cn; Fax: +86-27-87436235; Tel: +86-27-67883470

heavy metals ions. However, the amount of desired functional groups on the biochar surface that have sorption affinity for targeted heavy metals could be enhanced through different chemical routes.[11] Therefore, chemical modification by applying different chemical reagents is so far considered as a good alternative to enhance the adsorption capacity and selectivity for targeted pollutants as well as the stability of biochar-based metallic catalysts.[12]

A number of attempts have been made for biochar chemical modification in order to boost the adsorption capacity towards targeted pollutants. However, these methods use chemical reagents that are not environment-friendly such as harsh acids and bases.[13,14] Recently, it has been confirmed that the use of peroxides, such as H_2O_2, for the partial oxygenation of BC could enhance its cation exchange capacity due to the formation of more acidic OFGs, particularly carboxylic groups (–COOH) on the biochar surface.[15,16] These biochar-based –COOHs having slightly acidic nature activate in neutral or basic solutions and carry an overall negative charge, which is considered as a favorable environment for cation interaction through an adsorption mechanism. Xue et al.[17] also confirmed the effectiveness of H_2O_2-treated hydrochar (carbon rich material obtained through biomass by hydrothermal conversion) having enhanced adsorption capacity for metals ions from solution than that of the non-treated hydrochar. Both the strong oxidation ability and relatively low cost as well as the environment-friendly nature of H_2O_2 chemical reagent with final decomposition into clean products, namely, H_2O and O_2 make its application attractive in different fields. In addition, biochar-based functional groups such as carboxyl, amino, and hydroxyl groups also facilitate the anchoring or chemical grafting of other functional groups in order to get good performance and selectivity towards the removal of targeted pollutants. For example, $C \equiv N$ group-grafted biochar was successfully produced at a low pyrolysis temperature for enhancing the removal of cadmium from water.[18] Yang et al.[13] applied severe chemical conditions for the amino modification of biochar to enhance the adsorption capacity of copper ions. Moreover, in order to enhance the adsorption performance of rare earth elements (REEs) from water, polyethylenimine-cross-linked cellulose nanocrystals were successfully developed.[19] In another study, a novel multifunctional fluorescence-magnetic biochar was synthesized, which had very good magnetic properties along with the capability to remove pathogenic superbugs and toxic metals from an environmental water sample.[20] Recently, a combined amino and thiol group-functionalized multi-walled carbon nanotube (MWCNT) was successfully synthesized for Hg(II) ions adsorption from both synthetic and real wastewater aqueous solutions.[21] Furthermore, a successfully prepared mercaptoamine-functionalized silica-coated magnetic nanoadsorbent exhibited highly effective removal of both Hg(II) and Pb(II) ions from wastewater. Multiple adsorption sites (sulfur and amine sites) were present on the adsorbent surface, which accelerated the effective removal of both Hg(II) and Pb(II) ions.[22] Hence, it was confirmed that different chemical modification routes result in the formation of different functional groups on the biochar surface. They may be either

acidic OFGs, amino or thiol groups.[23] Thus, the above-mentioned studies gave us a direction to introduce multifunctional groups (–COOH and amino groups) on a biochar surface at the same time through the following steps: (i) partial-oxidation of biochar by applying H_2O_2 reagent; (ii) grafting of the amino functional groups onto the pre-oxidized biochar (BC–COOH) through the chemical activation of available –COOH groups; and (iii) observing the possible effects of one functional group on another functional group's performance with the main objective of Hg(II) adsorption from aqueous solution. Here, the selection of amine groups for the biochar modification was due to their relatively higher reactivity and selectivity towards Hg(II) ion removal through the formation of complexes via chelation as well as their unique property of reacting easily with many other functional groups. Dual benefits of simultaneously available –COOH and grafted amino functional groups on the biochar surface were studied to compensate the passivation of the grafted NH_2 groups by unwanted H^+ ions, which further accelerated the activation of residual –COOH groups to serve as extra active sites for Hg(II) ion removal. Overall, the significance of OFGs and grafted amino functional groups available on biochar was evaluated.

In this study, amino-grafted modified biochars (AMBC) with different amine-to-biochar weight ratios were synthesized. Fourier transform infrared (FTIR), scanning electron microscope (SEM), and X-ray photoelectron spectroscopy (XPS) characterization techniques were conducted to study the physiochemical properties of the as-prepared adsorbent that directly affect the Hg(II) removal mechanism. A sequence of batch experiments was conducted to investigate the adsorption performance, adsorption kinetics, and isotherms in detail.

2. Materials and methods

2.1. Preparation of BC

Raw corncobs, which are waste agro-materials, first underwent grinding to obtain a particle size of less than 0.6 mm. The obtained feedstock of uniform size was subjected to carbonization in a tubular muffle furnace at 400 °C for 1 h with a heating rate of 10 °C min^{-1} under nitrogen atmosphere to get BC.

2.2. Biochar chemical modification

Chemical modification of BC was performed in two steps. The procedure reported by Huff et al.[15] was adopted with slight modification in the partial oxidation of BC by applying a strong oxidant (H_2O_2) treatment during the first step. The aim behind BC oxidation is to get maximum –COOH groups through the oxidation of primary hydroxyl groups on the BC surface. Briefly, a 1 g biochar/20 mL H_2O_2 solution ratio was treated with 30% w/w H_2O_2 in a 50 mL plastic centrifuge tube. Then, a capped 50 mL centrifuge tube was placed into a mechanical rotatory shaker and was shaken for 3 h at 150 rpm. After completing 3 h of shaking period, the sample was vacuum filtered and then washed with 4 × 100 mL portions of ultra-pure water to eliminate any extra H_2O_2. Finally, the samples were dried overnight in an electric drying oven at 105 °C, which was chosen from the

study reported by Huff *et al.*[15] The control experiments were conducted by using water instead of the H_2O_2 reagent.

BC–COOH obtained from the first step was amino-functionalized through the –COOH group activation by directly grafting them with amines in the second step. The amination of BC–COOH was performed by a dipping method. Amino-functionalization of biochar was performed according to the literature.[24,25] In a 100 mL beaker, an appropriate amount of NaOH, urea and ultra-pure water in a specific ratio (4.5 : 15 : 100 by weight) was dispersed and then, the mixture solution was kept in the refrigerator until it was pre-cooled to a temperature between −5 °C and −15 °C. After the mixture solution reached the desired cooling temperature, BC–COOH was soaked promptly into the pre-cooled solution under vigorous stirring for a period of 15 min at room temperature. Finally, a specific amount of diethylenetriamine (DETA) was mixed under vigorous stirring, and the reaction elapsed for 6 h at ambient temperature. The suspension was separated by vacuum filtration, rinsed with deionized water until a neutral pH leachate was obtained and finally dried overnight at 60 °C in a drying oven. The as-obtained sorbent was named AMBC. The amine-to-BC weight ratio concept was adapted from the recently performed study on the fabricated hybrid material where Pd was supported on diethylenetriamine-functionalized single-walled carbon nanotubes (SWCNT-DETA/Pd).[26] Three different amine-to-BC weight ratios were chosen: 9 : 1, 13.5 : 1, and 18 : 1. Correspondingly, the obtained products were marked as amino-BC1 (9 : 1), amino-BC2 (13.5 : 1), and amino-BC3 (18 : 1).

2.3. Characterization

SEM was performed to observe the biochar surface morphology. XPS analysis was performed to determine the surface elements of C, N, and O. Both BC and AMBC samples were subjected to oven drying in order to ensure a constant weight and then, FT-IR analysis was performed to confirm the variety of different functional groups available on the biochar surface. A range of 400–4000 cm^{-1} was set for FT-IR spectra analysis. Boehm titration was performed to determine the content of surface functional groups following the standardization procedure set by Goertzen *et al.*[27–29] This method depends on the presence of OFGs having different acidity potentials that can be neutralized by applying bases of various strengths. As a weak base, $NaHCO_3$ has the ability to neutralize only –COOH groups; Na_2CO_3 has the potential to neutralize both lactonic and –COOH groups at once, and NaOH has the power to neutralize all phenolic, lactonic, and –COOH groups simultaneously due to its strong basic nature. The molar value of each surface functional group was calculated by applying the different methods.

2.4. Sorption experiments

A stock solution of Hg(II) (1000 mg L^{-1}) was prepared by dissolving analytical grade $HgCl_2$ salt in deionized water. For all experiments the desired concentration of Hg(II) solutions having pH 5 ± 0.1 adjusted with 0.5 M NaOH or 0.5 M HCl were obtained by diluting the freshly prepared stock solution with deionized water. Batch experiments were performed using

100 mL Erlenmeyer flasks containing 50 mL of the Hg(II) solutions. The initial Hg(II) concentration range was 1–20 mg L^{-1}, which was in accordance with the commonly found range of industrial wastewater effluents. The Erlenmeyer flasks were agitated on a rotary shaker at 150 rpm and at room temperature (25 °C). For adsorption kinetic and isotherm studies, after each sampling time (60 min, 120 min, 240 min, 360 min, 540 min, 690 min, 810 min, and 930 min), the suspensions were filtered immediately by passing through 0.22 μm Whatman membrane filter and then used for analysis. In order to avoid errors, all the experiments were performed in triplicate, and the results were finalized by calculating the mean values.

2.5. Mathematical models

Kinetic and equilibrium sorption models were applied to the experimental data. Hg(II) amount adsorbed (q_e) by the sorbent surface was calculated by eqn (1) based on a mass balance approach, while the removal efficiency (%) was calculated by applying eqn (2).

$$q_e = \frac{(C_o - C_e)V}{w} \tag{1}$$

$$p = \frac{(C_o - C_e)}{C_o} \times 100\% \tag{2}$$

where C_o is the Hg(II) initial concentration, C_e (mg L^{-1}) is the Hg(II) concentration at the equilibrium stage, V (L) is the volume of solution in liters and w (g) is the adsorbent weight added during the experiments.

Mathematical models named pseudo-first-order and pseudo-second-order models were applied to simulate the kinetics of Hg(II) sorption on the sorbent surface.

$$\log(q_e - q_t) = \log q_e - \frac{k_1 t}{2.303} \text{(Pseudo-first-order)} \tag{3}$$

$$\frac{t}{q_t} = \frac{1}{k_2 q_e^2} \frac{t}{q_e} \text{(Pseudo-second-order)} \tag{4}$$

where q_e and q_t are the adsorbent sorption capacity (mg g^{-1}) at equilibria and time t, respectively. Moreover, k_1 and k_2 are the reaction rate constants (min^{-1} and g mg^{-1} min^{-1}) for the pseudo-first-order model and the pseudo-second-order model, respectively.

Famous isotherm models such as Langmuir and Freundlich were applied in this study to describe the adsorption behaviour of Hg(II) on the sorbent surface. The Langmuir model is best fitted in the case of monolayer sorption on a homogeneous surface without any further interaction between the adsorbed molecules. However, the Freundlich model is applied to nonimitative and reversible phase adsorption over a heterogeneous surface.

$$\frac{1}{q_e} = \frac{1}{q_{max}} + \frac{1}{q_{max} K_L C_e} \text{(Langmuir model)} \tag{5}$$

$$\log q_e = \log K_f + \left(\frac{1}{n}\right) \log C_e \text{(Freundlich model)} \tag{6}$$

where q_e (mg g^{-1}) is the solid-phase concentration of Hg(II) at the equilibrium stage, and q_{max} (mg g^{-1}) and K_L (L mg^{-1}) are the maximum sorption capacity and free energy of sorption, respectively. The parameter K_f is the Freundlich constant connected to the adsorption constant, while $1/n$ is related to the adsorption strength. The slope ($1/n$) and intercept (log K_f) of the plot between log q_e and log C_e give us the numerical value of n and K_f, respectively.

3. Results and discussion

3.1. Characterization of multi-functionalized biochar

SEM analysis was performed to identify the changes in the surface morphology and structure of the biochar before and after applying the modification process. Fig. 1 shows the SEM images of BC, BC–COOH, and amino-BC2 samples. It was revealed that both the BC–COOH and the amino-BC2 surfaces were relatively rougher than the BC surface, which was quite smooth in appearance. This could be attributed to the combined effect of conversion of the primary hydroxyl groups available on BC into –COOH groups as a result of the reaction with the strong oxidizing agent H$_2$O$_2$ during the first stage as well as successful grafting reaction in the biochar cellulose structure upon the addition of the DETA chemical reagent during the second stage. Moreover, it can be noticed from the

SEM images that less ash is present on the amino-BC2 surface than that on the non-modified BC surface due to the prevailing alkaline conditions during the modification pathway that may accelerate the dissolution of ash and available residual content.[30] Furthermore, in contrast to basic and acidic treatments on the biochar, which resulted in the dissolution and demineralization of the available minerals or ash, respectively, the H$_2$O$_2$ oxidation treatment only altered the OFGs on the BC–COOH surface without the demineralization and dissolution of ash or the available minerals, as depicted by the presence of ash in the SEM image for the BC–COOH sample (Fig. 1(b)).[31]

XPS analysis confirmed the variations in BC surface elemental composition after the entire amino modification route. Fig. 2(a) shows the broad XPS scan for BC, BC–COOH, amino-BC2, and amino-BC2-Hg(II). C content for BC (81.1%), BC–COOH (78.2%), and amino-BC2 (76.35%), O-content for BC (18.05%), BC–COOH (21.25%), and amino-BC2 (15.86%), and N-content for BC (0.6%), BC–COOH (0.4%), and amino-BC2 (7.07%) were monitored. An increase in the O-content was noticed for BC–COOH when compared with that for BC sample, which confirmed biochar-surface oxygenation after H$_2$O$_2$ treatment. The peak shifting pattern, as shown in Fig. 2(b), for the O 1s full spectra confirms the conversion of the biochar surface's available hydroxyl groups into a different variety of OFGs, which was further supported by Boehm titration data given in Table 1.
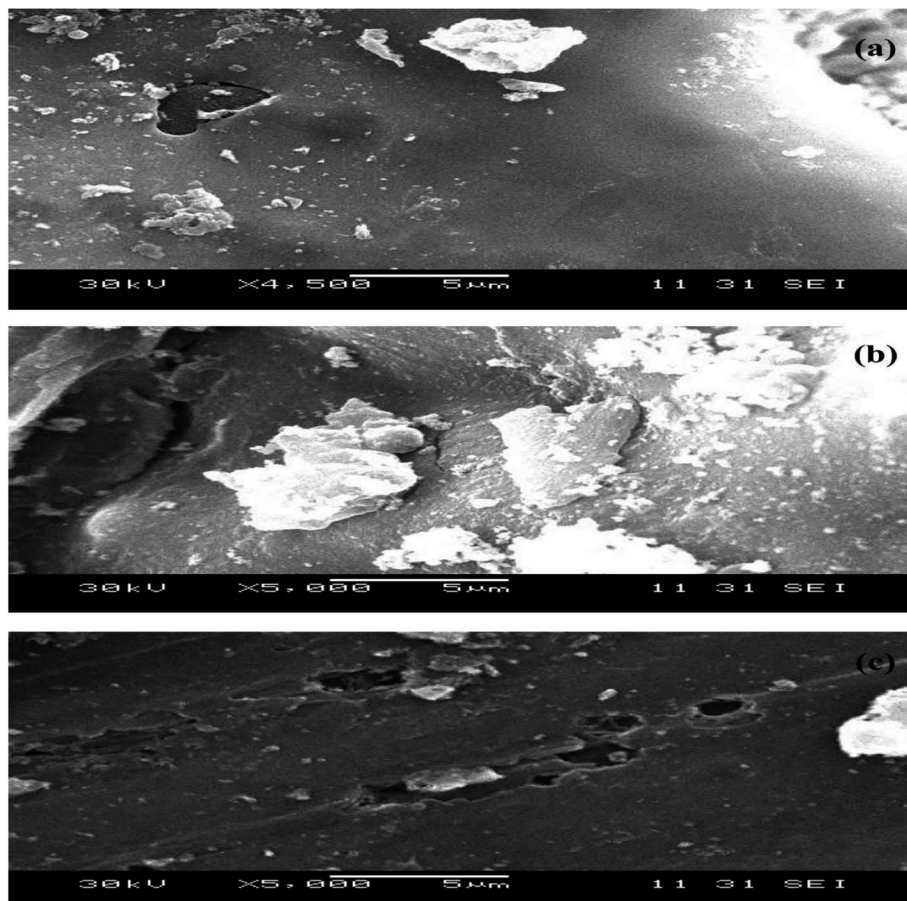

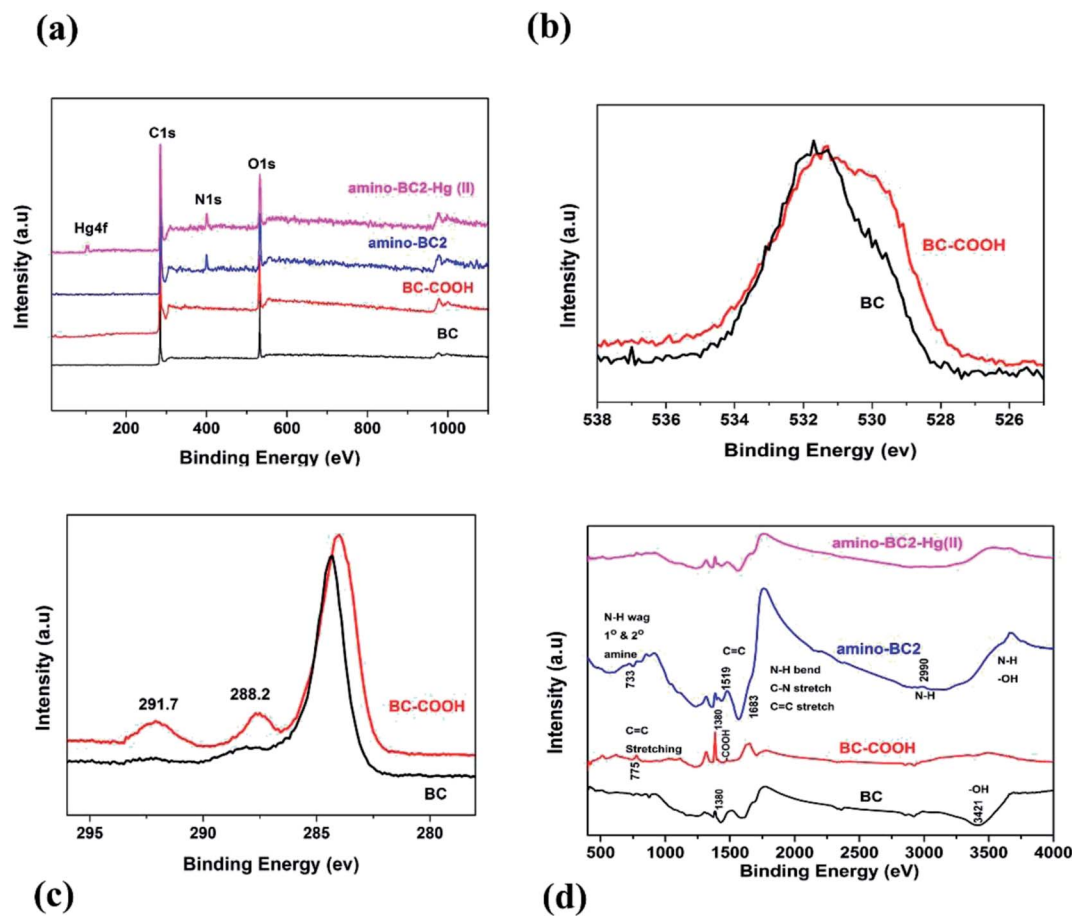Fig. 1 SEM images of BC (a), BC–COOH (b), and amino-BC2 (c).

Fig. 2 XPS wide scans of BC, BC−COOH, amino-BC2, and amino-BC2-Hg(II) (a), O 1s spectra of BC and BC−COOH (b), C 1s spectra of BC and BC−COOH (c), and FTIR spectra of BC, BC−COOH, amino-BC2, and amino-BC2-Hg(II) (d).

The literature data show that the peaks originating at 530.7 eV (carbonyl or quinone), 532.0 eV (ethers or hydroxyl), and 533.3 eV (lactone or carboxylic) as a result of the deconvolution of O 1s spectra were attributed to associated OFGs.[32] By a comparison of the BC and BC−COOH full O 1s spectra, given in Fig. 2(b), it was confirmed that most of the hydroxyl groups were converted into carboxylic, lactonic, carbonyl, and ether groups as a result of H$_2$O$_2$ treatment. Moreover, in the C 1s full spectra, as shown in Fig. 2(c), the peaks observed at about 288.2 eV and 291.7 eV for BC−COOH can be attributed to the

contribution of ketone functionality and π–π* transition, respectively.[33] The addition of carboxyl groups on BC surface as a result of H$_2$O$_2$ treatment, the electron density was removed from the π band of the carbon (π–π* transition) of the BC; thereby no contribution expected as a reducing environment due to the involvement of a π electron.[15] However, in the case of AMBC, the increase in the N content supported the successful amino grafting by −COOH group activation. The decrease in the O content can be explained by the biochar −COOH group attachment with amino-functional groups. Furthermore, Table

Table 1 Amount of surface groups calculated by Boehm titration and the Hg(II) removal efficiency of BC, BC−COOH, and AMBC

| Sample | Functional groups (mmol g^{-1}) | | | Total basic sites (mmol g^{-1}) | Experimental initial pH | Hg(II) removal (%) |
	Carboxylic (mmol g^{-1})	Phenolic (mmol g^{-1})	Lactonic (mmol g^{-1})			
BC	0.86	0.45	0.28	0.21	5	47.3
BC−COOH	1.95	0.21	0.33	0.39	5	40.9
Amino-BC1	0.53	—	N.D.^{a}	1.45	5	84.7
Amino-BC2	0.39	—	N.D.	1.56	5	97.6
Amino-BC3	0.16	—	N.D.	1.62	5	68.5

^{a} N.D.: not detectable.

1 shows that the results for the contents of acidic and basic surface functional groups on the biochar surface determined by the Boehm titration method were also in good agreement with the XPS measurements. Moreover, the data showing the acidic and basic surface functional group contents obtained by the Boehm titration method also confirmed the simultaneous existence of both grafted amino functional groups and residual –COOH groups on the biochar surface. Adsorption experiments were performed to judge the potential ability of the as-prepared AMBC samples for Hg(II) removal from aqueous solution. A series of different amine-to-BC weight ratio materials such as amino-BC1, amino-BC2 and amino-BC3 along with BC as well as BC–COOH were tested for Hg(II) removal. It was clear from the Hg(II) removal potential of all sorbents, as shown in Table 1, that the amination of biochar results in the relatively higher removal of Hg(II) ions than that obtained using BC. In particular, in the amino-BC3 sample, the efficiency of the Hg(II) ion removal decreased sharply despite the availability of the maximum total basic functional groups on the amino-BC3 surface. This might be due to the saturation of NH_2 basic sites with more competitive positive ions (H^+) than Hg(II) ions in aqueous solution (which will be discussed later in detail). Therefore, the amino-BC2 sample was considered for further investigation. The FTIR spectrum study was performed to obtain the functional groups available on the sorbent surface. As shown in Fig. 2(d), the broad and strong band lies in the range of 3419–3413 cm^{-1}, which could be attributed to the stretching vibrations of –OH and –NH groups.[34] The adsorption band positioned at 1683 cm^{-1} was assigned to C=O stretching vibrations of carbonyl from the abundant –COOH groups in biochar or the –NH–C=O from grafted amino groups after biochar modification with the DETA chemical reagent.[19,34,35] The band at 1380 cm^{-1} was attributed to the –COOH stretching vibrations in biochar, which normally disappeared in case of activated carbons having the properties of highest carbonation and lowest oxygen ratio.[30,36] Moreover, the bands at around 775 cm^{-1} and 733 cm^{-1} were attributed to the stretching vibrations of C=C in biochar and the N–H wagging mode due to successful biochar amination, respectively. The FTIR spectra before and after the adsorption of Hg(II) by amino-BC2 confirm the involvement of both –COOH groups and NH_2 basic sites for sorption removal of Hg(II) ions present in aqueous solution, which was reflected by the decrease in the intensity of peaks at 3421 cm^{-1}, 1683 cm^{-1}, 1380 cm^{-1}, and 733 cm^{-1}, which were assigned to the associated functional groups as described above.

3.2. AMBC performance evaluation towards Hg(II) sorption

Kinetic study is one of the key aspects used to examine how a reaction proceeds. A kinetic examination of equilibrium data gives us details about the residence time required for metal adsorption. Biochar-based Hg(II) sorption experiments were performed at pH 5 by monitoring the distribution of mercury species in an aqueous system as a function of pH. In addition, to avoid the removal of Hg(II) ions through the precipitation process, the change in the final pH was monitored during the

protonation of amino-functional groups, which was counter-balanced in the later stages (saturation and equilibrium phases) due to the de-protonation of the remaining or residual –COOH functional groups on the biochar surface. Fig. 3(a) shows that both BC and BC–COOH exhibit comparatively less sorption of Hg(II) ions, with a removal efficiency of 47.3% and 40.9%, respectively. The relatively less sorption observed for BC–COOH as compared with that of BC might be due to less or no activation of the acidic nature of –COOH groups at pH 5.[15] However, a kinetic study of amino-BC2 confirmed that during the first 1 h of reaction rapid initial sorption was observed, resulting in the removal of 77.6% of Hg(II) ions after the saturation phase was reached, and the equilibrium point was finally reached after 810 min. An increase in pH was observed (pH$_{initial}$: 5.0 → pH$_{final}$: 6.11, Fig. 3(b)), which was assigned to the protonation effects on nitrogen atoms of the amino-functionalized biochar. Thus, the maximum active binding sites on the amino-functionalized biochar were diminished during the competitive adsorption phase between Hg(II) and H^+ ions within the initial 2 h of the reaction. Following this, a slight decrease in pH was noticed, which might be due to the activation of residual –COOH groups on the biochar surface. The –COOH groups possessed a slightly acidic nature. The activation of –COOH occurred in neutral or basic aqueous solutions, which resulted in the biochar carrying an overall negative charge to favorably interact with Hg(II) ions.[32] Hence, the subsequent sorption of the Hg(II) ions until the equilibrium stage was due to the contribution of residual –COOH groups. Therefore, in this study, it was observed that the passivation of the NH_2 groups by the interaction with Hg(II) and H^+ resulted in the activation of residual –COOH groups, which further contributed as the active sites for the Hg(II) sorption. Moreover, for the amino-BC1 and amino-BC3 samples, the Hg(II) ion removal efficiency decreased to 84.7% and 68.5%, respectively, as shown in Fig. 3(c). The decrease in the removal efficiency might be due to a relatively smaller amount of grafted amino functional groups available in the case of amino-BC1, which could be attributed to the lower amount of DETA utilized for the modification purpose. However, more protonation of the relatively excess grafted amino functional groups was noticed, as depicted by an increase in the pH value (pH$_{initial}$: 5.0 → pH$_{final}$: 6.11) in the case of amino-BC3, which could be assigned to a higher dosage of DETA applied for the chemical modification. These obtained results were in agreement with the acidic and basic group data obtained from the Boehm titration technique, given in Table 1. In addition, the as-prepared highly efficient amino-BC2 was also applied for a variety of toxic metals to confirm its selectivity and efficiency for different metal ions sorption. It was observed that amino-BC2 exhibited maximum removal efficiency (97.6%) for Hg(II) ions than for Cu(II) (62.3%), Zn(II) (51.7%), and Pb(II) (38.9%), as shown in Fig. 3(d). This might be due to the tendency of different metals ions to interact with different functional groups differently.[37,38] The observed change in the removal efficiency for different metal ions can be described by the electronegativity values of the metal ions under consideration. The metal adsorption sequence should follow the same order as their electronegativities, which are Pb (2.33),
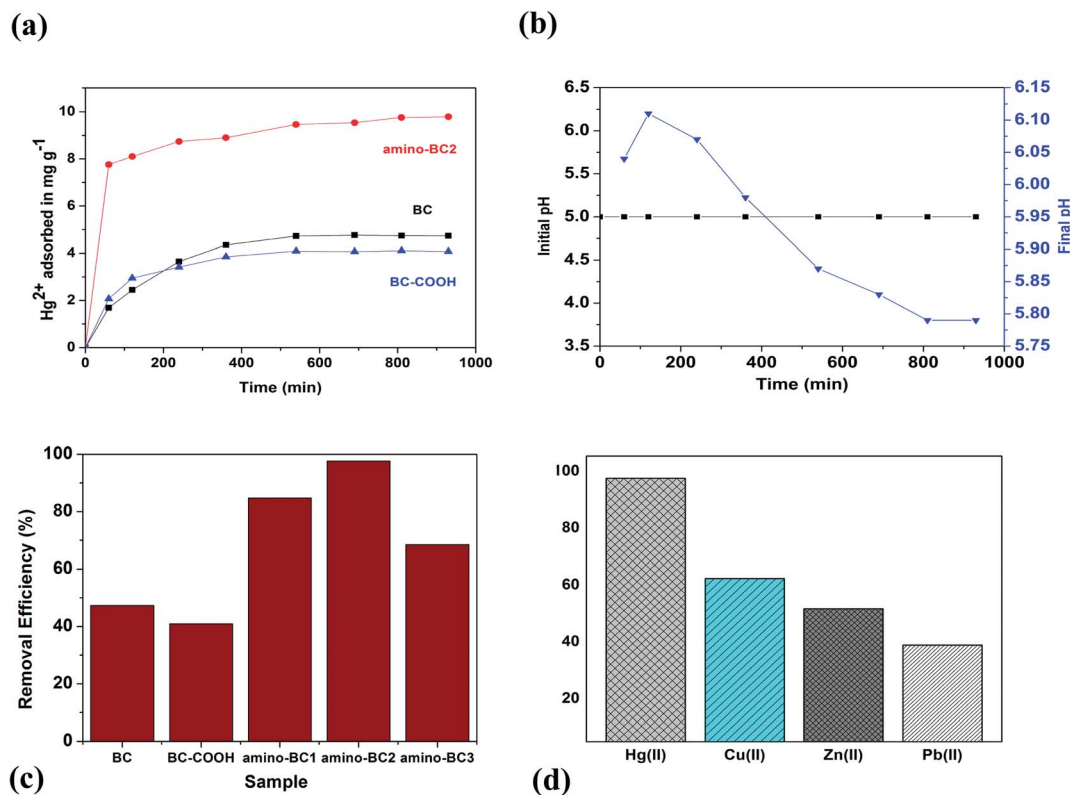
Fig. 3 Hg(II) sorption by BC, BC–COOH, and amino-BC2 (a). Initial pH variation for amino-BC2 (b). Performance evaluation of BC, BC–COOH, and AMBC (c). Amino-BC2 selectivity towards different metals ions (d).

Hg (2.00), Cu (1.90), and Zn (1.65).[39] However, lead, despite its higher electronegativity value, was one of the least-removed cations during the monometal adsorption study in our case. Similar findings were reported in the literature, in which cadmium, despite its lower electronegativity value, was one (except for Pb) of the most retained cations in the monometal adsorption study.[40] However, there might be another factor behind the change in the removal efficiency for different targeted metal ions noticed in our study, which could be considered for a future research study. In addition, the experimental adsorption data were further analyzed through the two most commonly used kinetic approaches: pseudo-first-order (eqn (3)) and pseudo-second-order (eqn (4)). The fitted adsorption kinetics parameters for amino-BC2 and BC are given in Table 2. The kinetics study data, given in Fig. 4(a) and (b), best fitted to pseudo-second-order, as depicted by the relatively high value of the regression coefficient (R^2) for BC (0.995) and amino-BC2 (0.999). Moreover, a relatively slight difference was observed in between q_e (cal) and q_e (exp) for the pseudo-second-order than the pseudo-first-order. Commonly, a larger sorption rate constant k_1 indicates quicker adsorption, whereas a small k_2 value is assigned to faster adsorption. However, in our case, the k_2 value for amino-BC2 was higher than the k_2 value for BC. The higher k_2 value reflects that amino-BC2 had more surface hydrophobicity than BC (having a smaller k_2 value). This might be attributed to the removal of soluble carbon (SC) from BC

(<500 °C) during the amino-functionalization in alkaline solution. A recently performed study observed a similar trend for the sorption rate constant k_2 when base-modified biochars were applied for phenanthrene sorption.[30] In addition, the hydrophobicity for both biochar samples was measured in terms of the water contact angle (CA) by using the Wilhelmy plate method.[41] The calculated values of CA for BC and amino-BC2 were 111 ± 1 and 117 ± 2, respectively. The increase in the CA value from 111 ± 1 to 117 ± 2 reflects the higher hydrophobicity for amino-BC2 than that for BC sample. These results were in agreement with the sorption rate constant (k_2) values for both BC and amino-BC2.

The phenomenon governing the movement or release of adsorbate from the liquid phase to solid surface media can be

Table 2 Pseudo-first-order and pseudo-second-order kinetics parameters for sorption of Hg(II) on BC and amino-BC2 at 25 °C

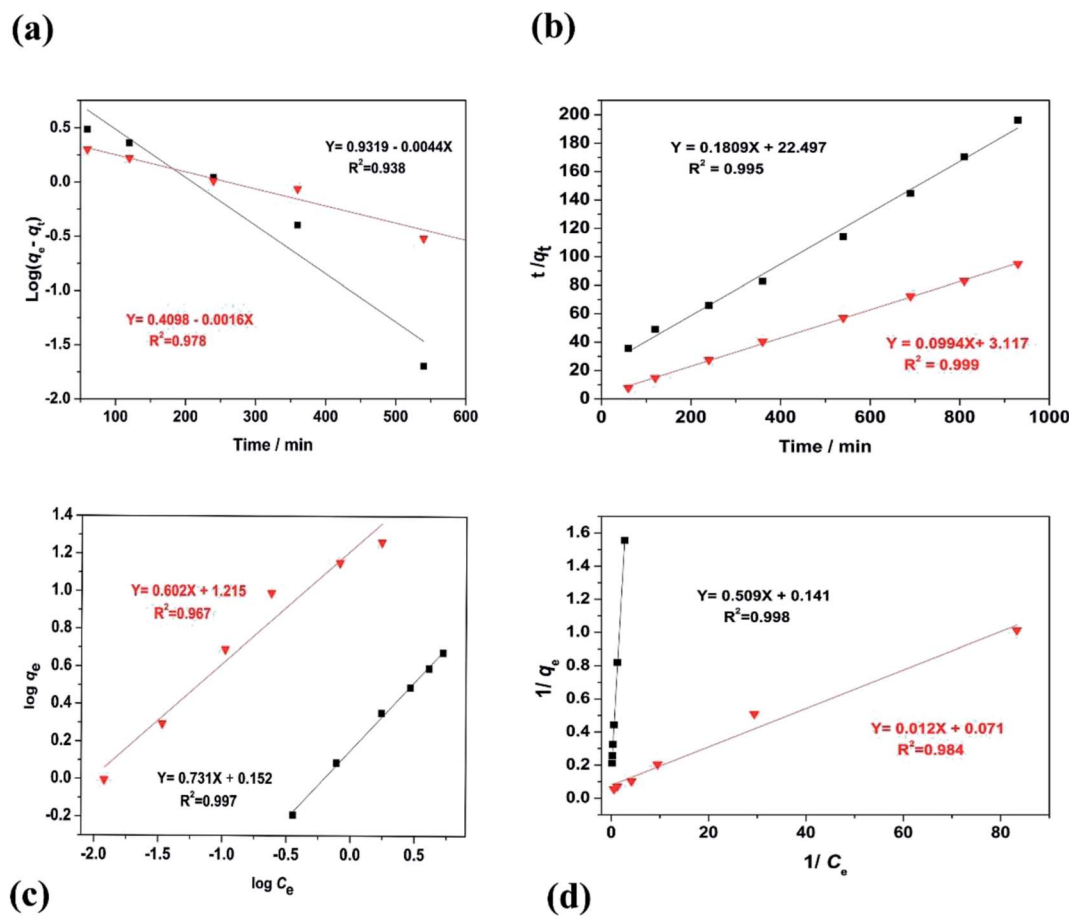| Kinetic model	Parameters	Amino-BC2	BC
Pseudo-first order	$q_{e(cal)}$ (mg g^{-1})	2.57	8.55
	$q_{e(exp)}$ (mg g^{-1})	9.76	4.75
	k_1 (min^{-1})	4.0×10^{-3}	10×10^{-3}
	R^2	0.978	0.938
Pseudo-second order	$q_{e(cal)}$ (mg g^{-1})	10.06	5.53
	$q_{e(exp)}$ (mg g^{-1})	9.76	4.75
	k_2 (g mg^{-1} min^{-1})	3.2×10^{-3}	1.4×10^{-3}
	R^2	0.999	0.995

Fig. 4 For BC and amino-BC2: pseudo-first-order model fitting (a), pseudo-second-order model fitting (b), Freundlich isotherm fitting (c) and Langmuir isotherm fitting (d).

expressed by employing adsorption isotherms. The most common isotherms model, namely, Langmuir (eqn (5)) and Freundlich (eqn (6)) models were used in this study to investigate the adsorption of $Hg(II)$ by BC and amino-BC2 sorbents.

For both BC and amino-BC2 sorbents, the isotherms of $Hg(II)$ sorption were well-explained by applying a linear model ($R^2 >$ 0.96). Fig. 4(a) and (b) show that both the Langmuir and Freundlich were best fitted models since they adequately describe the $Hg(II)$ sorption data, as depicted by the higher value of regression coefficient (R^2) near or close to the value 1 (Table 3). The Langmuir adsorption constant (K_L) for BC and amino-BC2 were 0.28 L mg^{-1} and 6.13 L mg^{-1}, respectively. The higher value of K_L for amino-BC2 might be attributed to the presence of both –COOH and grafted amino groups on the modified biochar surface, which were mostly accepted as the

main contributors for the coordination between $Hg(II)$ ions and sorbent surface media. In addition, in the case of the Freundlich model, the value of n was 1.37 and 1.66 for BC and amino-BC2, respectively. If n values lie in the range in between one and ten, favorable sorption occurred. According to the Langmuir model, by using the data from the intercept and slope of the plot of $1/C_e$ versus $1/q_e$, the parameters K_L and q_{max} were calculated as 14.1 mg g^{-1} and 6.13 L mg^{-1}, respectively. The calculated q_{max} value for amino-BC2 was almost twice that of BC, which was 7.1 mg g^{-1}. These findings confirm that biochar surface functionalization enhanced the adsorption capacity.

Moreover, the adsorption capacity (q_{max}) of the studied amino-BC2 for $Hg(II)$ ions was compared with other literature-based adsorbents and summarized in Table 4. For example, the guava bark- and walnut shell-activated carbon

Table 3 Adsorption isotherm models for $Hg(II)$ sorption and corresponding parameters

Adsorbent	Langmuir			Freundlich		
	q_{max} (mg g^{-1})	K_L (L mg^{-1})	R^2	K_f (mg^{1-n} L^n g^{-1})	n	R^2
BC	7.1	0.276	0.998	1.42	1.37	0.997
Amino-BC2	14.1	6.13	0.984	16.42	1.66	0.967

demonstrated the maximum adsorption capacity of 3.4 mg g^{-1} and 7.5 mg g^{-1}, respectively, which were comparable with that of BC in our study.[42,43] The coconut-button-waste-derived activated carbon exhibited good adsorption capacity for many heavy metals including Hg(II) ions (12.21 mg g^{-1}).[44] Recently, amino functionalized activated carbon labelled as the PEI-AC composite was synthesized,[45] and showed the interaction of amino groups with Hg(II) ions, as depicted by the high adsorption capacity of 16.39 mg g^{-1}. The q_{max} for amino-BC2 prepared in this study was 14.1 mg g^{-1}, which was comparable to the PEI-AC composite adsorption performance and higher than that of the literature-reported adsorbents derived from biochar as a raw material.[8,46] The q_{max} of the studied amino-BC2 for Hg(II) ions was lower than that of a few adsorbents, while it was higher than that for most of the listed adsorbents. However, in terms of economic and environmental aspects, AMBC could be considered as an attractive adsorbent.

In addition, desorption study was also performed to determine whether the biochar-sorbed or laden mercury could be recovered and recycled. The amino-BC2 sample that had already been utilized once for the sorption of mercury (0.5 g of the sample stirred for a duration of 24 hours to achieve maximum adsorption with 10 mg L^{-1} mercury solution at pH 6) was mixed with 100 mL of 10% HCl solution for 12 hours. It was revealed from the desorption experiments that it is possible to recover and recycle a fraction of biochar-sorbed mercury from the amino-BC2 sample. In the case of the reused amino-BC2 sample, only 47% of the mercury desorbed, which might be due to the limited concentration of the desorption agent.[47]

3.3. Mechanism overlaid Hg(II) sorption by AMBC

For the purpose of elucidating the adsorption mechanism of Hg(II) removal by AMBC, FTIR and XPS techniques were performed before and after adsorption experiments. As shown in Fig. 2(d), the shifting of peaks from 3584 cm^{-1} to 3456 cm^{-1} was assigned to the presence of –OH or –NH$_2$ stretching vibrations, while the decrease in intensity was monitored for the peaks positioned at 1683 cm^{-1} and 1380 cm^{-1}, which were attributed to NH bending and –COOH stretching vibrations,

respectively.[30,34] The shifting of peaks and decrease in peak intensity confirm the role of –OH, –NH$_2$, –NH and –COOH groups with Hg(II) ions present in aqueous solution. Furthermore, in the FTIR spectrum of BC–COOH, there was no peak observed at 1519 cm^{-1} (C=C), and relatively a sharp peak was found at 1380 cm^{-1} as compared with the untreated or BC FTIR spectra. This trend confirmed that the small amount of aromatic carbon in the BC sample was altered and also, the amount of –COOH groups increased as a result of H$_2$O$_2$ treatment.[15] In addition, a band at around 733 cm^{-1}, attributed to N–H wagging, was recorded for the amino-BC2 sample after amino-functionalization, which diminished for the amino-BC2-Hg(II) sample, which confirmed the contribution of –NH$_2$ groups in Hg(II) ion sorption.

XPS analysis was also performed to confirm the contribution of biochar surface functional groups for Hg(II) ion removal from aqueous solution. The full XPS spectrum and high-resolution XPS spectra for the amino-BC2 and amino-BC2-Hg(II) are given in Fig. 2(a) and 5(a–c), respectively. There were two typical strong peaks noted at 101.3 eV (Hg 4f $_{7/2}$) and 105.4 eV (Hg 4f $_{5/2}$), having a binding energy gap of 4.1 eV in the high-resolution spectra of Hg 4f (Fig. 5(a)). The peak noted at 101.3 eV was assigned to the Hg–O band.[48,49] These strong facts endorsed the hypothesis that Hg(II) was sorbed in the ionic form and not by the contribution of the precipitation reaction, and the crystal form was loaded on the amino-BC2 surface. Moreover, in Fig. 5(b) the N 1s high-resolution XPS spectra reflect only one peak at 399.3 eV (N–H or H–N–H) for amino-BC2. However, one additional peak was observed at 401.8 eV along with an already available peak at 399.3 eV for amino-BC2-Hg(II) (Fig. 5(c)), which was assigned to metal-N.[35] Therefore, these results confirm the contribution of both amino-grafted and residual –COOH groups towards Hg(II) sorption. In addition, there was no change in the C 1s peaks detected before and after the adsorption experiments, which revealed that no contribution by the reduction process (Hg(II) → Hg(I)) was observed due to the possibility of π-electrons in the biochar aromatic structure. Hence, it can be concluded that several interactions, namely, ion exchange, surface complexation, and electrostatic attraction were responsible for Hg(II) adsorption.

Table 4 Comparison of maximum adsorption capacities for Hg(II) exhibited by various adsorbents

| Adsorbent	q_{max} (mg g^{-1})	Experimental conditions			References
		Dosage (g mL^{-1})	pH	T (°C)	
Soybean stalk-based BC	0.7	0.01/30	7	25	8
Phragmites karka	1.79–2.27	1/100	7	25	46
Guava bark	3.4	1/100	9	30	42
Na$_2$S-modified corn straw BC	5.71	0.02/60	4	25	36
Walnut shell activated carbon	7.5–8.7	0.05/50	5	29	43
Coconut button activated carbon	12.5	0.1/50	7	30	44
PEI-AC composite	16.39	0.03/20	5	25	45
Modified microalgae residuals	62.5	0.01/30	5	30	50
BC	7.1	0.05/50	5	25	Our finding
Amino-BC2	14.1	0.05/50	5	25	Our finding
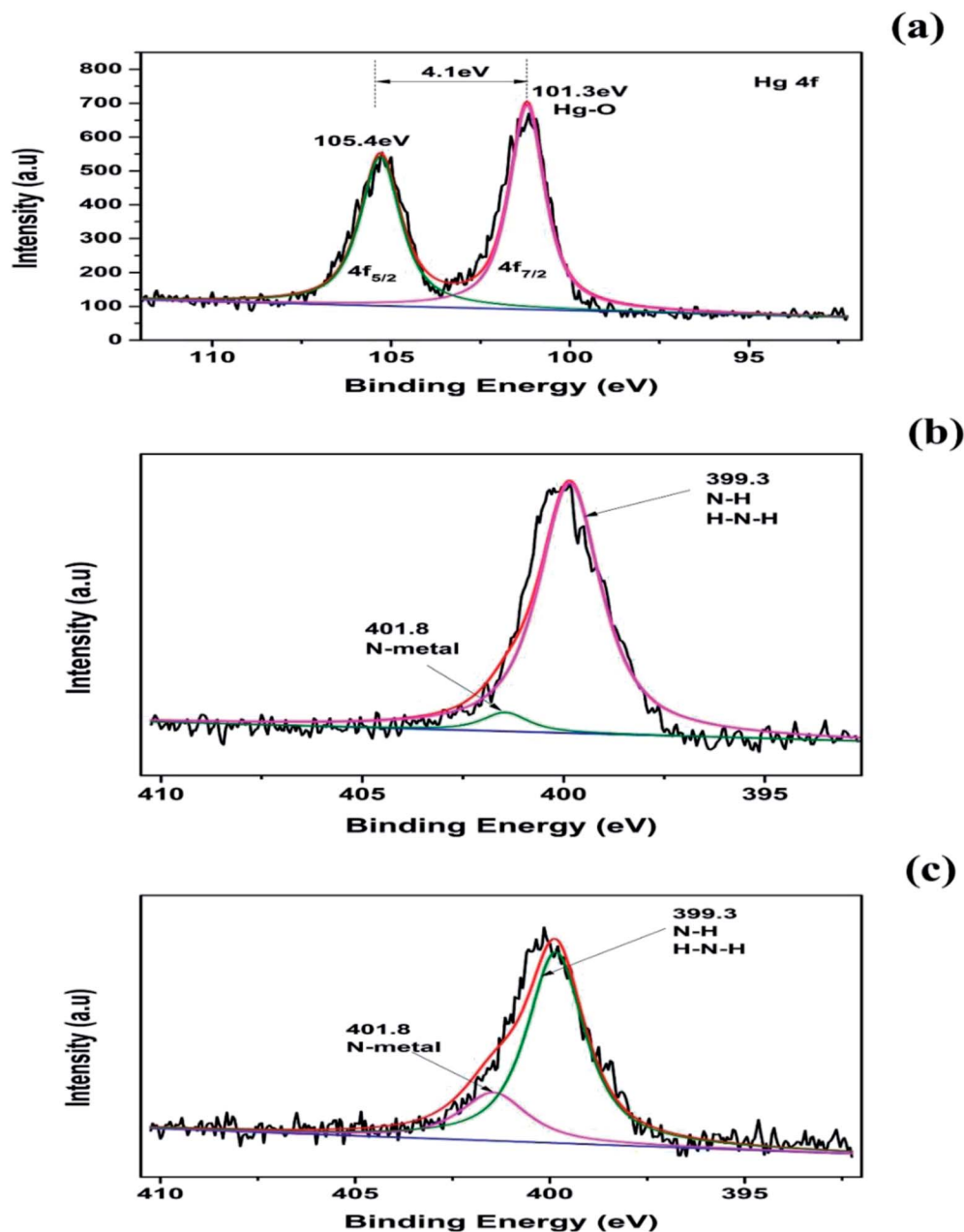
Fig. 5   High-resolution XPS spectra of amino-BC2: Hg 4f (a), N 1s before Hg(II) adsorption (b), and N 1s after Hg(II) adsorption (c).

4.   Conclusion

A new low-cost adsorbent, AMBC, was successfully synthesized by a novel approach, termed as the amination reaction between DETA and BC–COOH and applied for the detoxification of Hg(II) ions from aqueous solutions. The results confirm the effectiveness of the modification due to a significant improvement in the adsorption performance for Hg(II) ion removal from aqueous solutions. The increase in adsorption was attributed to the contribution of grafted amino and available residual –COOH groups on the adsorbent surface, which resulted in chemisorption only. It is also acknowledged that this facile synthetic route can provide more direction to develop a wide range of different functional biochar-based materials in various fields of application.

Conflicts of interest

There are no conflicts of interest to declare.

Acknowledgements

References

1 H. N. M. E. Mahmud, A. O. Huq and R. binti Yahya, *RSC Adv.*, 2016, **6**, 14778–14791.

2 A. Shokrollahi, M. Ghaedi and M. Shamsipur, *Quim. Nova*, 2009, **32**, 153–157.

3 L. Trasande, P. J. Landrigan and C. Schechter, *Environ. Health Perspect.*, 2005, **113**, 590.

4 J. H. Cai and C. Q. Jia, *Ind. Eng. Chem. Res.*, 2010, **49**, 2716–2721.

5 N. Pirrone, S. Cinnirella, X. Feng, R. B. Finkelman, H. R. Friedli, J. Leaner, R. Mason, A. B. Mukherjee, G. B. Stracher and D. G. Streets, *Atmos. Chem. Phys.*, 2010, **10**, 5951–5964.

6 A. Sharma, A. Sharma and R. K. Arya, *Sep. Sci. Technol.*, 2015, **50**, 1310–1320.

7 X. Xu, A. Schierz, N. Xu and X. Cao, *J. Colloid Interface Sci.*, 2016, **463**, 55–60.

8 H. Kong, J. He, Y. Gao, H. Wu and X. Zhu, *J. Agric. Food Chem.*, 2011, **59**, 12116–12123.

9 E. El-Shafey, *J. Hazard. Mater.*, 2010, **175**, 319–327.

10 H. Yu, J. Liu, J. Shen, X. Sun, J. Li and L. Wang, *J. Taiwan Inst. Chem. Eng.*, 2016, **66**, 313–320.

11 H. Huang, J. Tang, K. Gao, R. He, H. Zhao and D. Werner, *RSC Adv.*, 2017, **7**, 14640–14648.

12 W.-J. Liu, H. Jiang and H.-Q. Yu, *Chem. Rev.*, 2015, **115**, 12251–12285.

13 G.-X. Yang and H. Jiang, *Water Res.*, 2014, **48**, 396–405.

14 R. Azargohar and A. Dalai, *Microporous Mesoporous Mater.*, 2008, **110**, 413–421.

15 M. D. Huff and J. W. Lee, *J. Environ. Manage.*, 2016, **165**, 17–21.

16 J. W. Lee, A. Buchanan, B. R. Evans and M. Kidder, in *Advanced biofuels and bioproducts*, Springer, 2013, pp. 35–45.

17 Y. Xue, B. Gao, Y. Yao, M. Inyang, M. Zhang, A. R. Zimmerman and K. S. Ro, *Chem. Eng. J.*, 2012, **200**, 673–680.

18 M. Luo, H. Lin, B. Li, Y. Dong, Y. He and L. Wang, *Bioresour. Technol.*, 2018, **259**, 312–318.

19 F. Zhao, E. Repo, Y. Song, D. Yin, S. B. Hammouda, L. Chen, S. Kalliola, J. Tang, K. C. Tam and M. Sillanpää, *Green Chem.*, 2017, **19**, 4816–4828.

20 Y. Gao, A. Pramanik, S. Begum, C. Sweet, S. Jones, A. Alamgir and P. C. Ray, *ACS Omega*, 2017, **2**, 7730–7738.

21 M. Hadavifar, N. Bahramifar, H. Younesi and Q. Li, *Chem. Eng. J.*, 2014, **237**, 217–228.

22 S. Bao, K. Li, P. Ning, J. Peng, X. Jin and L. Tang, *Appl. Surf. Sci.*, 2017, **393**, 457–466.

23 D. O'Connor, T. Peng, G. Li, S. Wang, L. Duan, J. Mulder, G. Cornelissen, Z. Cheng, S. Yang and D. Hou, *Sci. Total Environ.*, 2018, **621**, 819–826.

24 C. Jiang, H. He, X. Yao, P. Yu, L. Zhou and D. Jia, *J. Appl. Polym. Sci.*, 2018, **135**, 45759.

25 A. El-Khouly, E. Kenawy, A. Safaan, Y. Takahashi, Y. Hafiz, K. Sonomoto and T. Zendo, *Carbohydr. Polym.*, 2011, **83**, 346–353.

26 R. Ghorbani-Vaghei, S. Hemmati, M. Hashemi and H. Veisi, *C. R. Chim.*, 2015, **18**, 636–643.

27 A. M. Oickle, S. L. Goertzen, K. R. Hopper, Y. O. Abdalla and H. A. Andreas, *Carbon*, 2010, **48**, 3313–3322.

28 S. L. Goertzen, K. D. Thériault, A. M. Oickle, A. C. Tarasuk and H. A. Andreas, *Carbon*, 2010, **48**, 1252–1261.

29 G. Peng, F. Gramm, C. Ludwig and F. Vogel, *Catal. Sci. Technol.*, 2015, **5**, 3658–3666.

30 Z. Feng and L. Zhu, *Front. Environ. Sci. Eng.*, 2018, **12**, 1.

31 X. Cui, S. Fang, Y. Yao, T. Li, Q. Ni, X. Yang and Z. He, *Sci. Total Environ.*, 2016, **562**, 517–525.

32 X. Dong, L. Q. Ma, Y. Zhu, Y. Li and B. Gu, *Environ. Sci. Technol.*, 2013, **47**, 12156–12164.

33 Z. Li, L. Wu, H. Liu, H. Lan and J. Qu, *Chem. Eng. J.*, 2013, **228**, 925–934.

34 M.-m. Zhang, Y.-g. Liu, T.-t. Li, W.-h. Xu, B.-h. Zheng, X.-f. Tan, H. Wang, Y.-m. Guo, F.-y. Guo and S.-f. Wang, *RSC Adv.*, 2015, **5**, 46955–46964.

35 W. Liang, M. Li, Z. Zhang, Y. Jiang, M. K. Awasthi, S. Jiang and R. Li, *Int. J. Biol. Macromol.*, 2018, **113**, 106–115.

36 G. Tan, W. Sun, Y. Xu, H. Wang and N. Xu, *Bioresour. Technol.*, 2016, **211**, 727–735.

37 J. H. Park, J. S. Cho, S. O. Yong, S. H. Kim, S. W. Kang, I. W. Choi, J. S. Heo, R. D. Delaune and D. C. Seo, *Environ. Lett.*, 2015, **50**, 1194–1204.

38 J. H. Park, Y. S. Ok, S. H. Kim, J. S. Cho, J. S. Heo, R. D. Delaune and D. C. Seo, *Chemosphere*, 2016, **142**, 77–83.

39 M. McBride, *Environmental chemistry of soils*, Oxford Univ. Press, New York, 1994.

40 J.-H. Park, Y. S. Ok, S.-H. Kim, J.-S. Cho, J.-S. Heo, R. D. Delaune and D.-C. Seo, *Chemosphere*, 2016, **142**, 77–83.

41 S. Bubici, J. P. Korb, J. Kučerik and P. Conte, *Magn. Reson. Chem.*, 2016, **54**, 365–370.

42 M. B. Lohani, A. Singh, D. Rupainwar and D. Dhar, *J. Hazard. Mater.*, 2008, **159**, 626–629.

43 M. Zabihi, A. H. Asl and A. Ahmadpour, *J. Hazard. Mater.*, 2010, **174**, 251–256.

44 T. Anirudhan and S. Sreekumari, *J. Environ. Sci.*, 2011, **23**, 1989–1998.

45 T. A. Saleh, A. Sarı and M. Tuzen, *J. Environ. Chem. Eng.*, 2017, **5**, 1079–1088.

46 M. H. Raza, A. Sadiq, U. Farooq, M. Athar, T. Hussain, A. Mujahid and M. Salman, *J. Chem.*, 2015, **2015**, DOI: 10.1155/2015/293054.

47 A. M. Rizzuti, F. L. Ellis, L. W. Cosme and A. D. Cohen, *Mires and Peat*, 2015, **16**, 1–7.

48 J. Wilcox, E. Sasmaz, A. Kirchofer and S.-S. Lee, *J. Air Waste Manage. Assoc.*, 2011, **61**, 418–426.

49 G. Li, B. Shen, Y. Wang, S. Yue, Y. Xi, M. An and K. Ren, *Fuel*, 2015, **145**, 189–195.

50 Y. Peng, X. Liu, X. Gong, X. Li, Y. Liu, E. Leng and Y. Zhang, *Energy Fuels*, 2018, **32**, 4461–4468.